ACS APPLIED MATERIALS & INTERFACES

Research Article

www.acsami.org

# Selective Optical Response of Hydrolytically Stable Stratified Si Rugate Mirrors to Liquid Infiltration

Tero Jalkanen,*[,†,‡] Vicente Torres-Costa,[§] Ermei Mäkilä,[†] Martti Kaasalainen,[†] Ryo Koda,[‡] Tetsuo Sakka,[‡,∥] Yukio H. Ogata,[‡] and Jarno Salonen[†,⊥]

[†]Department of Physics and Astronomy, University of Turku, FI-20014 Turku, Finland

[‡]Institute of Advanced Energy, Kyoto University, Uji, Kyoto 611-0011, Japan

[§]Departamento de Fisica Applicada, C-XII, Universidad Autónoma de Madrid, Cantoblanco, 28049 Madrid, Spain

[∥]Department of Energy and Hydrocarbon Chemistry, Graduate School of Engineering, Kyoto University, Nishikyo-ku, Kyoto 615-8510, Japan

[⊥]Turku University Centre for Materials and Surfaces, University of Turku, FI-20014 Turku, Finland

Supporting Information

**ABSTRACT:** Stratified optical filters with distinct spectral features and layered surface chemistry were prepared on silicon substrates with stepwise anodic porosification and thermal carbonization. The use of differing parameters for successive carbonization treatments enabled the production of hydrolytically stable porous silicon-based layered optical structures where the adsorption of water to the lower layer is inhibited. This enables selective shifting of reflectance bands by means of liquid infiltration. The merit of using thermal carbonization for creating layered functionality was demonstrated by comparing the hydrolytic stability resulting from this approach to other surface chemistries available for Si. The functionality of the stratified optical structures was demonstrated under water and ethanol infiltration, and changes in the adsorption properties after 9 months of storage were evaluated. The changes observed in the structure were explained using simulations based on the transfer matrix method and the Bruggeman effective medium approximation. Scanning electron microscopy was used for imaging the morphology of the porous structure. Finally, the adaptability of the method for preparing complex structures was demonstrated by stacking superimposed rugate structures with several reflective bands.

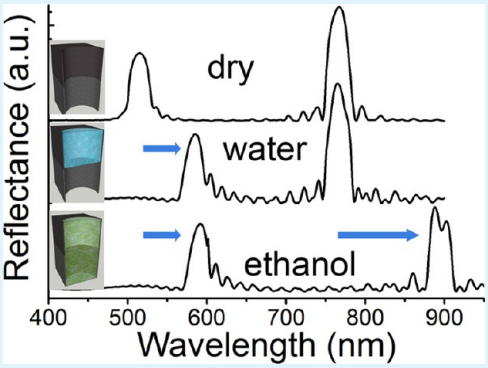


**KEYWORDS:** *porous silicon, rugate filter, hydrolytic stability, photonic crystal, chemical modification, thermal carbonization*

## INTRODUCTION

Monitoring the properties of liquids is of interest in many applications, such as environmental sensing. For example, in biosensing and microfluidic applications, it is often desirable to receive information about the properties of liquid analytes and the possible changes that occur in them.[1−3] Moreover, in these types of applications, sample volumes are sometimes small, making miniaturization of the sensing element a high priority. Optical detection, based on observing the changes in the optical path length of a nanoporous film or mirror, is a simple and non-destructive method for monitoring the properties of liquid or gaseous analytes infiltrating the pores. Nanostructured silicon (i.e., porous Si, PSi) is a high-surface-area material with controllable optical properties and is in many ways optimal for sensing applications.[4−7] The adjustable fabrication with electrochemical anodization enables facile preparation of a variety of dielectric mirrors such as rugate filters and other 1D photonic crystals.[8−10] Additionally, the applicability of PSi in optical detection of gases and vapors has been established.[4] Furthermore, PSi has also proven to be useful in biosensing applications that take place in the liquid phase.[11] However, due to the large internal surface area, PSi is prone to hydrolytic corrosion in aqueous solutions, making it too unreliable and unstable for long-term applications.[12,13] Simple chemical stabilization methods, such as thermal oxidation or hydrosilylation, are sometimes sufficient for guaranteeing an acceptable level of stability in gas-sensing applications.[13,14] However, if our interest lies in monitoring optical changes that take place in the liquid phase, then the situation changes considerably.

The nanostructured Si surface can be shielded against hydrolysis by attaching Si−C-bonded chemical species to it. This increased stability is attributed to the strength and low polarity of the Si−C bond.[15] Although partial Si−C coverage can be achieved with hydrosilylation methods, thermal carbonization (TC) is more viable a method for creating

Received: November 28, 2013
Accepted: January 22, 2014
Published: January 22, 2014

  

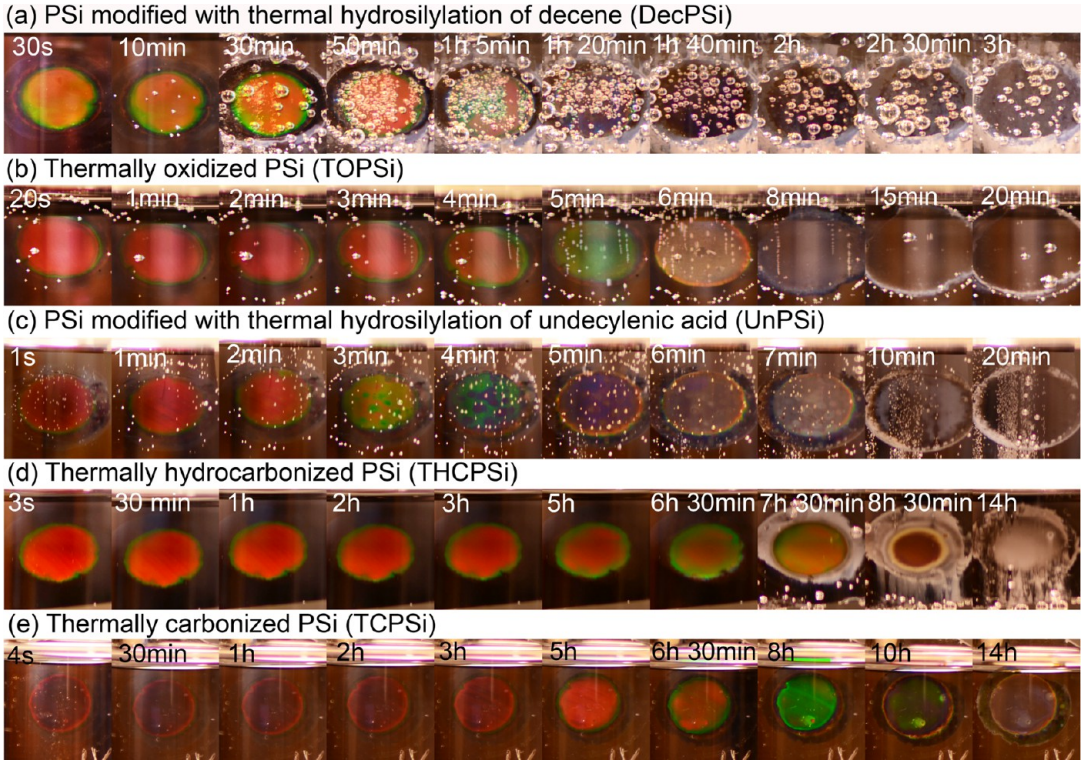


**Figure 1.** Temporal evolution of differently modified PSi reflectors immersed in 1 M NaOH and recorded with time-lapse photography: (a) DecPSi, (b) TOPSi, (c) UnPSi, (d) THCPSi, and (e) TCPSi. The brightness and contrast in individual photographs have been slightly modified to make the figure as clear as possible. Note the difference in the time scales.

robust surfaces because it allows for better coverage and considerably higher hydrolytic stability. The carbonization treatment is also flexible, as it enables the creation of hydrophobic or hydrophilic surfaces.[16,17] In addition, the suitability of TC in stabilizing optical filters has been demonstrated.[13,18] Therefore, TC enables the preparation of dual filters with hydrophilic and hydrophobic functionality, similar to the ones demonstrated by the group of Prof. Sailor.[19,20] However, the advantage of using TC is that the dual filters are hydrolytically stable enough for long-term applications in the liquid phase. Even though proof-of-concept studies involving microparticles in the liquid phase have been published before,[19] a PSi-based optical filter displaying dual functionality and acceptable long-term stability in aqueous media has not been shown to date.

In the current study, we describe a method for producing stratified optical filters with layered functionality from PSi. Although the basic principle is the same as in previous proof-of-concept studies, we were able to extend the life-span of these structures far beyond the levels achievable with conventional methods by using thermal carbonization for stabilizing the surface. As a result, the structures are stable enough for actual use in applications involving repeated liquid infiltration with only slight and predictable changes in optical functionality. This makes activation of PSi-based passive optical elements with fluidic infiltration feasible. In addition, we demonstrate that the method can be used for preparing more complex filters, where interesting new phenomena, such as adsorption-induced splitting of a reflectance band, can be achieved in a controlled manner.

## RESULTS AND DISCUSSION

**Chemical Stability in Aqueous Media.** The surface of PSi offers diverse possibilities for chemical modification.[15,21−23] Modification of the chemical composition of the nanostructured Si surface provides control over the adsorption of molecules inside the porous layer and also greatly affects the hydrolytic stability of the material.[14] In Figure 1, the differences in hydrolytic stability for varying surface chemistries are illustrated under accelerated conditions. PSi optical mirrors were first treated with thermal hydrosilylation of 1-decene or undecylenic acid, thermal oxidation, thermal hydrocarbonization, and thermal carbonization, respectively, and submerged in a 1 M aqueous NaOH solution. The chemical-etch rate in alkaline solutions depends on, among other things, the surface termination of the Si surface. For example, the etch rate of SiC is orders of magnitude smaller than that of thermal oxide.[24] Furthermore, the high specific surface area of PSi accelerates the rate of corrosion significantly.

From Figure 1b, we can see that the thermally oxidized PSi mirror dissolves completely in less than 20 min. Moreover, there is a big difference in the corrosion resistance of PSi mirrors that were modified by grafting hydrocarbon chains, namely, undecylenic acid or 1-decene, to the surface. The 1-decene-modified mirror is rendered useless after a little more than a 1 h soak, whereas the undecylenic acid-modified mirror dissolves much faster. The difference is most probably due to the hydrophobic character of the 1-decene-modified surface, which slows the hydrolytic corrosion because the surface is not wetted upon contact with water. However, hydrolytic stability is greatly increased by treating the surface with thermal carbonization (TC) or thermal hydrocarbonization (THC) (Figure 1e,d). Even though the stability of hydrosilylated and


dx.doi.org/10.1021/am405436d | ACS Appl. Mater. Interfaces 2014, 6, 2884−2892

carbonized surfaces is based on employing strong Si−C bonds, steric hindrance complicates bonding of long hydrocarbon chains to the silicon surface. As a result, hydrosilylation methods result in lower surface coverage and inferior hydrolytic stability. In thermal carbonization, however, carbon atoms diffuse into the silicon walls, creating a protective silicon carbide layer, which is more robust than mere monolayer coverage. Thermal hydrocarbonization results in a high-coverage $C_xH_y$ decorated surface, which is hydrophobic. The high coverage in THC can be attributed to the small size of the acetylene molecule used in the treatment.

The hydrolytic stability of TCPSi is especially astonishing, as the hydrophilic mirror does not completely dissolve in 1 M NaOH even after 14 h (Figure 1e). This is in stark contrast to the poor stability displayed by other hydrophilic PSi surfaces shown in Figure 1b,c. Additionally, for the hydrophobic surface terminations, we notice a clear distinction in the hydrolytic corrosion resistance in favor of the thermally hydrocarbonized surface (Figure 1a,d).

In light of these results, the merit of using TC and THC treatments for creating stratified optical filters with layered functionality should be obvious. Even though dual filters with hydrophilic and hydrophobic filter layers have been demonstrated for PSi before,[19,20] the results shown in Figure 1 demonstrate that the hydrolytic instability renders them useless for long-term applications involving liquid infiltration. In the following sections, we will demonstrate how stratified optical filters can be prepared from PSi utilizing TC and THC treatments and how the optical response can be selectively manipulated with liquid infiltration.

**Preparation of Stratified Optical Filters with Layered Functionality.** The basic principle for making layered PSi structures utilizing the TC/THC treatment is demonstrated here by preparing simple structures, where two single-band rugate filters[25−27] are prepared in succession, one on top of the other. The schematic flow of the process is presented in Figure 2a. The process begins by preparation of the first rugate filter on Si by means of anodization in a HF-based electrolyte. The newly prepared filter is then removed from the electrochemical cell, dried, and stabilized by thermal carbonization at 700 °C. The stabilized TCPSi filter is placed back in the electrochemical cell, and a second filter is anodized below the first one. Owing to the stability of the Si−C bonds, the carbonized surface is inert to excessive dissolution in HF, thus enabling anodization of a second filter below the TCPSi layer. The TCPSi surface resembles a SiC surface, and dipping TCPSi in HF merely removes the surface oxide, resulting in a stable hydroxyl surface termination.[28−30] After the second anodization, the lower filter can be stabilized by treating the sample with a thermal hydrocarbonization (THC) treatment conducted at 500 °C. This process results in a stratified TC/THC optical structure, where the upper filter layer is hydrophilic and the lower layer is, conversely, resistant to water infiltration because of the hydrophobic nature of the THCPSi surface. Figure 2b shows a cross-sectional SEM micrograph of a stratified TC/THC structure composed of two stacked single-band rugate filters. Both layers produce a distinctive peak in the reflectance spectrum (Figure 2c). The spectral positions of the peaks depend on the average refractive index and the period of the sine wave used in the respective refractive-index profiles. Quintic refractive-index matching layers are incorporated to the air-PSi and PSi-Si interfaces because they have been proven to reduce sidelobe intensity in the reflectance spectrum.[31,32] The

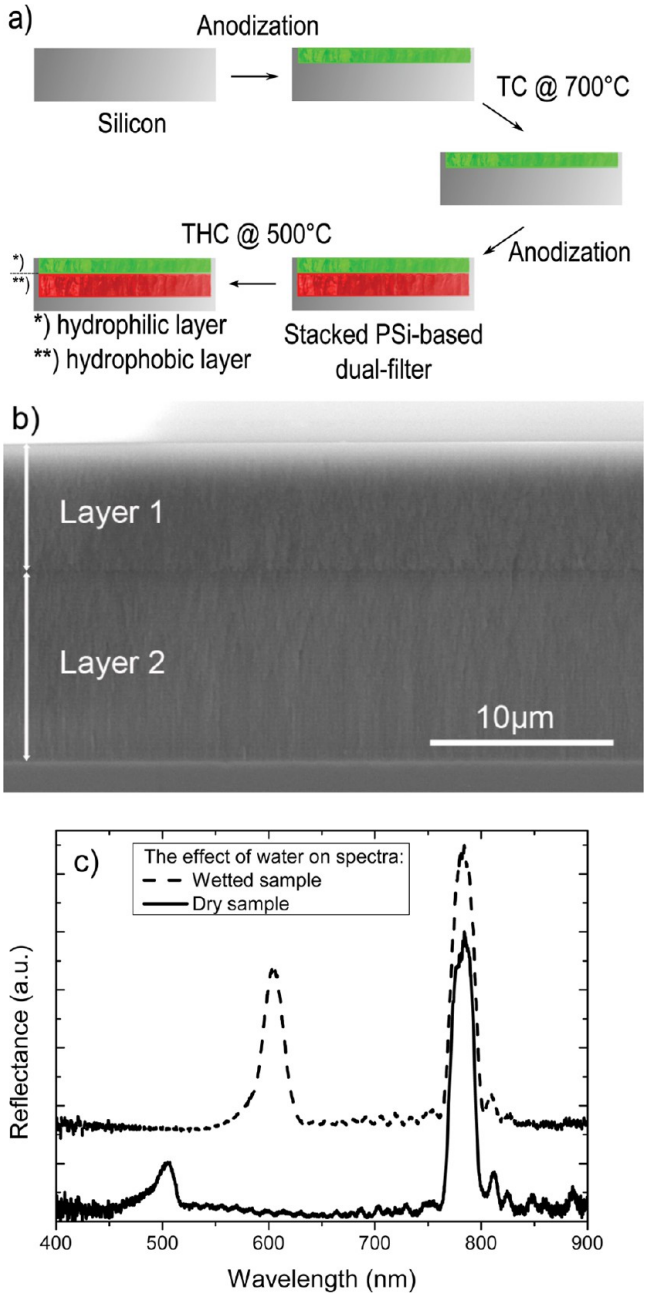


**Figure 2.** Schematic presentation of the preparation process for stacked rugate filters with TC/THC surface chemistry (a). A cross-sectional scanning electron micrograph of a TC/THC stacked rugate filter (b). The upper TCPSi layer (layer 1) is hydrophilic, whereas the lower THCPSi layer is hydrophobic. This can be seen clearly in the reflectance spectra measured for the TC/THC rugate filter in air (lower spectrum) and when the filter surface is wetted with water (upper spectrum) (c). The spectra are shifted vertically for clarity.

functionality of the TC/THC structure is demonstrated in Figure 2c, where a clear red shift is seen for the reflectance band related to the hydrophilic TCPSi filter as the structure is fully wetted with water. It should also be noted that the position of the second reflectance band, related to the lower hydrophobic THCPSi layer, remains unchanged. This is because water is unable to infiltrate the pores on the lower filter.

**Long-Term Performance and Aging Effects.** The long-term performance of stratified TC/THC rugate filters were investigated by storing the samples under ambient conditions

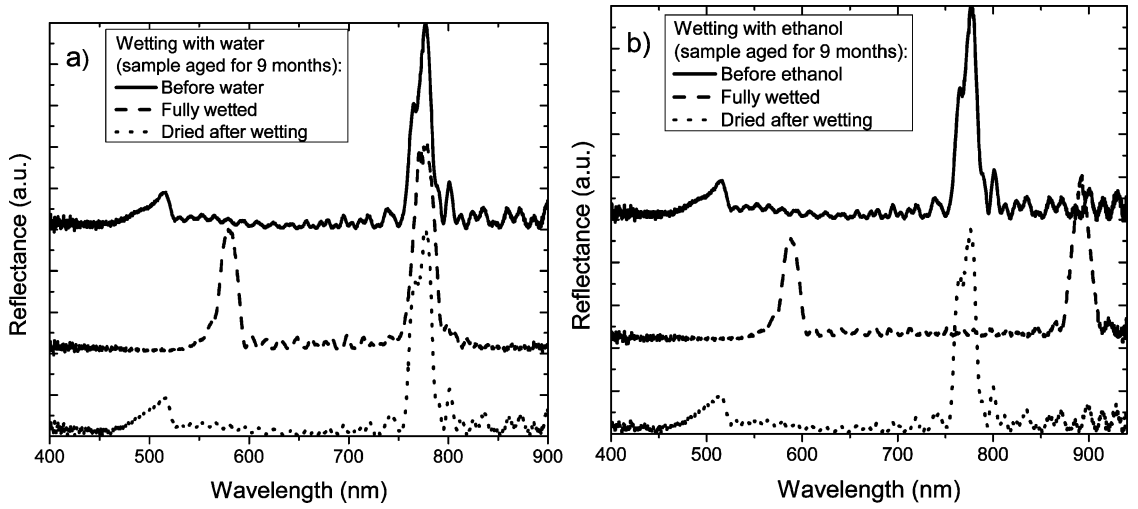


**Figure 3.** Functionality of a sample aged for 9 months when subjected to water (a) or ethanol (b). Water infiltrates only the upper TCPSi filter layer, whereas ethanol fills the entire structure. Therefore, both reflectance bands experience a red shift when the rugate structure is wetted with ethanol. The spectra are shifted vertically for clarity.

for a period of 9 months. Surface oxidation of the upper TCPSi layer was expected to cause changes in the adsorption properties of the upper filter.[13] The functionality of an aged sample is shown in Figure 3. We can see that the functionality of the stratified structure remains unchanged (i.e., water infiltrates the upper filter but is unable to advance to the THCPSi layer; Figure 3a). However, upon inspecting the magnitude of the red shift caused by fluidic infiltration, we noticed that the reflectance band does not shift as much compared to a freshly prepared sample (shifted peak position of approximately 580 vs 605 nm for the freshly prepared sample). This aging is attributed to surface oxidation of TCPSi, which reduces the amount of accessible pore volume and might also render some of the pores inaccessible to water. The aging effect can be replicated with simulations, and is discussed in more detail later. Even though the magnitude of the red shift is reduced, the functionality remains, and the adsorption-induced red shift is fully reversible even for aged samples. In other words, the reflectance band returns to the initial position upon water desorption.

Wetting the sample with ethanol causes a shift in both reflectance bands (Figure 3b) (shifted peak positions of approximately 588 and 892 nm). This is expected because ethanol is able to fully infiltrate the pores throughout the whole stratified structure. We also see that the ethanol-induced shift, observed for the first band, is slightly larger than in the case of water infiltration. We attribute this to the larger optical refractive index of ethanol, which causes a more prominent increase in the effective refractive-index value. Finally, we see that the process is fully reversible also for ethanol, and the shape of the reflectance spectrum is restored after evaporation of the liquid.

**Simulations.** To clarify the effects caused by the aging phenomenon, the experimental results were compared to simulated spectra. The simulated spectra were calculated with the transfer matrix method.[33] We began with simplified simulations by neglecting the effects caused by optical absorption and dispersion. The Bruggeman effective medium approximation (EMA)[34,35] was used to obtain the effective refractive index values for porous silicon. The two-component version of the Bruggeman EMA is a good starting point, and it takes the following form

$$p\frac{n_{\mathrm{fill}}^2 - n_{\mathrm{eff}}^2}{n_{\mathrm{fill}}^2 + 2n_{\mathrm{eff}}^2} + (1-p)\frac{n_{\mathrm{Si}}^2 - n_{\mathrm{eff}}^2}{n_{\mathrm{Si}}^2 + 2n_{\mathrm{eff}}^2} = 0 \quad (1)$$

where $p$ is the porosity (the porous volume fraction), $n_{\mathrm{fill}}$ is the optical refractive index of the material filling the pores, $n_{\mathrm{Si}}$ is the refractive index of silicon, and $n_{\mathrm{eff}}$ is the effective refractive index of PSi. Here, we also make the simplifying assumption that the pore walls in TCPSi have the same refractive index as bulk silicon. Although a thin non-stoichiometric silicon carbide layer is formed on the TCPSi pore walls and SiC has a lower refractive index than Si, experimental results have shown that the effective refractive index of TCPSi is only slightly smaller than the refractive index of as-anodized PSi.[18] In the case of THCPSi, the difference in the refractive indices is even smaller. The refractive index used for Si in the simulations ($n_{\mathrm{Si}} = 3.93$) was acquired using the Sellmeier equation. The corresponding Sellmeier coefficients were obtained from the online database for refractive indices.[36] Refractive-index values at a wavelength of 589 nm were used because the first reflectance band is situated close to this region.

Figure 4 shows the simulated spectra for the stratified rugate structure when we assume a sinusoidal porosity variation. This assumption should be a fair estimate for a restricted porosity range.[37] We could alternatively assume a strictly sinusoidal refractive-index variation, and the differences in the simulated spectra with this simplification would be very small (Figure S1). The period length for the sinusoidal modulation of the PSi rugate filters was estimated from SEM images (152 nm for the upper filter and 228 nm for the lower filter). The refractive-index values were calculated with the Bruggeman EMA for all porosities. The average porosity used in the simulations was $p = 0.685$ for both filter layers, and the amplitudes for sinusoidal porosity variation were 0.026 and 0.013 for the upper and lower layers, respectively. Prominent sidelobes are obvious in the first round of simulations. However, the intensity can be clearly reduced by adding refractive-index matching layers to the air-PSi and PSi-Si interfaces, as seen in the second-round simulations (Figure 4). The effect that the refractive-index matching layers have on PSi morphology at the PSi-Si interface

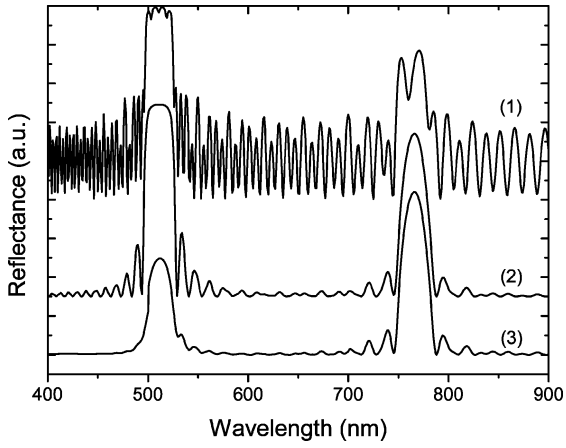


**Figure 4.** Reflectance spectra simulated with the transfer matrix method. The porosity is assumed to change linearly with anodization current, and the corresponding refractive index values were calculated with the Bruggeman EMA. Reflectance spectra are shown for a sample composed of two rugate filters stacked on top of each other (1), two rugate filters with quintic refractive index matching layers on the air-PSi and PSi-Si interfaces (2), and two rugate filters with quintics and a dispersive extinction coefficient used for the upper rugate layer (3).

can be inspected with SEM imaging (Figure S2). Finally, we adjusted the reflectance band intensity by taking optical absorption into account by using a discretely dispersive extinction coefficient, $k$, for the upper TCPSi layer (Figure S3). This approximation was used in place of a continuously dispersive $k$ because it simplifies the simulation but does not affect the simulated optical red-shift values that will be presented later. As a result, we end up with a simulated spectrum with the reflectance bands in the right wavelength regions and intensities corresponding to the experimental results. The shape of the simulated spectrum is similar to the experimental one (Figure 2c), even though the experimental spectrum displays more prominent optical absorption below 600 nm. The intensity of the first reflectance band in our simulation could be further reduced by making the extinction coefficient values larger.

We can now test the effect of filling the upper TCPSi layer with water by calculating a new refractive-index profile where the refractive index of air ($n$ = 1), used for the fill-component, $n_{\mathrm{fill}}$, in the two-component Bruggeman EMA, is replaced by that of water ($n_{\mathrm{H_2O}}$ = 1.330). Because the reflectance band originating from the upper filter layer is located around 600 nm, we used the refractive-index values at a wavelength of 589 nm for all the fill components. Figure 5a shows the simulated reflectance spectrum for a stratified TC/THC filter wetted with water. We can see that the simulations correspond well with the experimental results obtained with a freshly prepared sample (Figure 2c). However, by looking at Figure 3, it is evident that some modifications are needed to account for the aging effects. The aging phenomenon can be explained by the growth of a thin oxide layer on the inner surface of the TCPSi layer.[13,29]

If we want to account for aging, we need to incorporate a component describing the oxide layer into the simulations. For this, we applied the generalized Bruggeman EMA. For spherical inclusions, the generalized Bruggeman equation takes the following form[38]

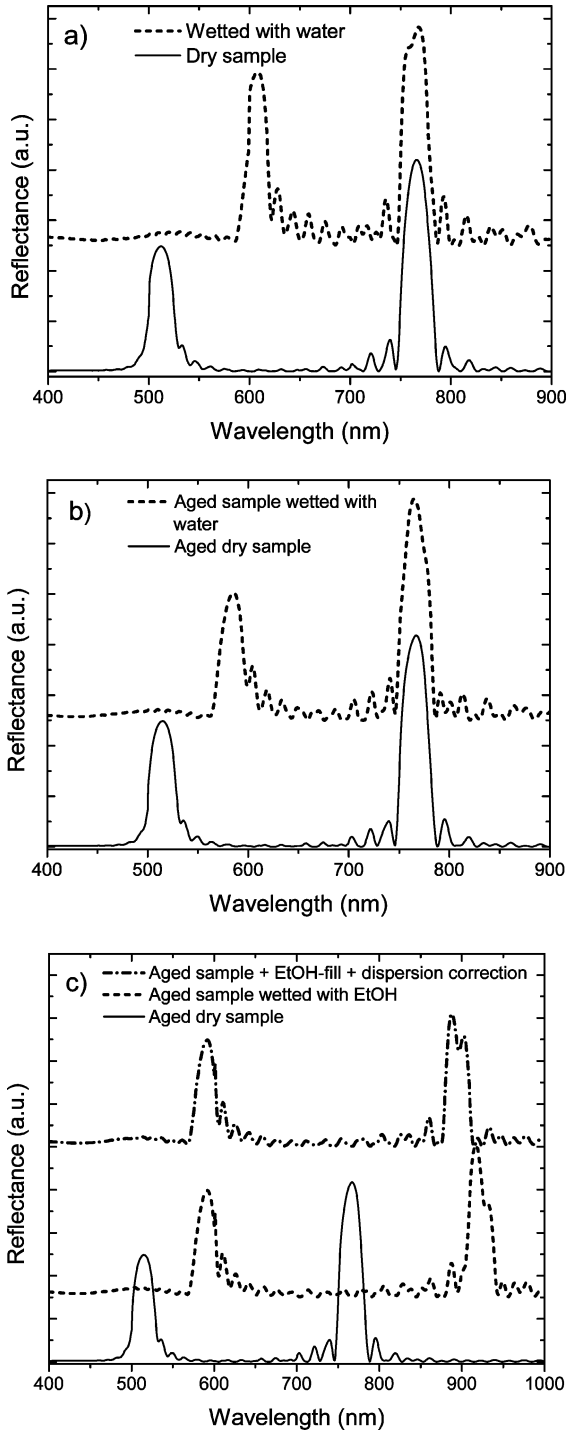


**Figure 5.** Simulated reflectance spectra for porous rugate structures in air and when wetted with water or ethanol. Freshly prepared sample with and without water infiltration (a). Aged sample with an oxide layer with and without water infiltration (b). Aged sample with and without ethanol infiltration as well as with ethanol infiltration when refractive-index dispersion is taken into account with a simple correction (c).

$$\sum_{i=1}^{m} f_i \frac{n_i^2 - n_{\mathrm{eff}}^2}{n_i^2 + 2n_{\mathrm{eff}}^2} = 0 \qquad (2)$$

where $f_i$ is the volume fraction of component $i$ and $n_i$ is the respective refractive index. If we now assume that a thin oxide layer is grown on the TCPSi layer, then the Bruggeman


dx.doi.org/10.1021/am405436d | ACS Appl. Mater. Interfaces 2014, 6, 2884−2892

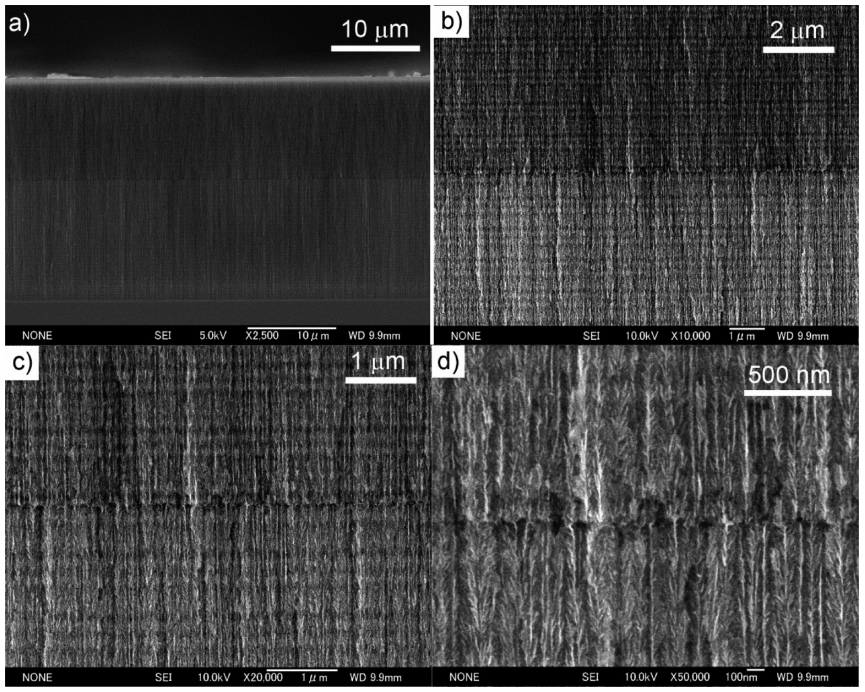


**Figure 6.** Cross-sectional SEM images of a stratified TC/THC optical structure composed of two superimposed rugate filters on top of each other: the entire structure at 2500× magnification (a) and the interfacial region at 10 000× (b), 20 000× (c), and 50 000× magnification (d).

formula, describing the composite medium, takes the following three-component form

$$d\frac{n_{ox}^2 - n_{eff}^2}{n_{ox}^2 + 2n_{eff}^2} + (p - d)\frac{n_{fill}^2 - n_{eff}^2}{n_{fill}^2 + 2n_{eff}^2} + (1 - p)\frac{n_{Si}^2 - n_{eff}^2}{n_{Si}^2 + 2n_{eff}^2} = 0 \quad (3)$$

where $d$ is the volume fraction of the oxide layer in the porous matrix and $n_{ox}$ is the corresponding refractive index. Because we assume that the oxide layer is formed on the surface of TCPSi and therefore does not penetrate into the carbonized pore walls, the volume fraction of the silicon skeleton remains unchanged. However, the oxide layer takes space from the pores, and as a result, we end up with a new term $(p - d)$, which describes the remaining pore fraction not filled with the oxide. For the simulations, we used the refractive-index value of silica to describe the oxide layer, $n_{ox} = n_{SiO_2} = 1.46$. It should be noted that the model does not take into account the fact that a small amount of Si atoms from the skeleton are required for the formation of the oxide layer. However, this approximation is justified because the change in the Si skeleton volume is small enough to not have any relevant effects to the simulation results.

Next, we needed to find an estimate for the volume fraction, $d$, describing the oxide layer. We can do this by comparing reflectance spectra for freshly prepared and 9 month-old samples. For three samples, we found that the reflectance peak from the TCPSi layer underwent an average red shift of 3.2 nm over the course of 9 months. If we attribute this red shift to the formation of an oxide layer, we find, by repeating the reflectance simulations with eq 3, that it corresponds to an approximate volume fraction $d \approx 0.01$. Finally, we need to make one more assumption to simulate the wetting behavior of the aged samples successfully. It is plausible to assume that the oxide layer may block some of the smaller pores, thus rendering them inaccessible to liquid infiltration. To account for this in our simulations, we needed to employ a four-component version of the Bruggeman EMA

$$b\frac{n_{b,air}^2 - n_{eff}^2}{n_{b,air}^2 + 2n_{eff}^2} + d\frac{n_{ox}^2 - n_{eff}^2}{n_{ox}^2 + 2n_{eff}^2} + (p - d - b)\frac{n_{fill}^2 - n_{eff}^2}{n_{fill}^2 + 2n_{eff}^2} + (1 - p)\frac{n_{Si}^2 - n_{eff}^2}{n_{Si}^2 + 2n_{eff}^2} = 0 \quad (4)$$

where $b$ is the volume fraction of pores in the matrix blocked from infiltration, and $n_{b,air}$ is the refractive index for air blocked inside. Here, the newly formed term $(p - d - b)$ describes the fraction of pores still accessible to liquid infiltration. If we now repeat our simulation, then by calculating the refractive-index profile with eq 4 using the values $d = 0.01$ and $b = 0.2$, we find that our simulation, for the water-infiltrated sample (Figure 5b), matches the experimental result for the aged sample (Figure 3a) quite well. Even though a blockage fraction of 0.2 sounds surprisingly large, it coincides well with nitrogen sorption results, demonstrating that the accessible pore volume of TCPSi can increase from a value of 0.87 to 1.04 $cm^3/g$ after the surface oxide is removed with a HF dip.[29]

Finally, we simulated the spectrum for a sample infiltrated with ethanol. A refractive-index value of $n_{EtOH} = 1.3614$ was used for ethanol. In this case, the lower THCPSi layer will also be wetted, so the refractive-index profile for the TCPSi layer needs to be calculated with the four-component Bruggeman EMA, whereas for the lower THCPSi layer, we can use eq 1. When simulating the spectra (Figure 5c), we found that the shift for the TCPSi-related reflectance peak matches the experimental result (Figure 3b) quite accurately. However, the peak shift related to the filling of the THCPSi layer is too large. This discrepancy can be attributed to optical dispersion. All refractive-index values used in the simulations are for wavelengths below 600 nm and therefore do not accurately reproduce optical shifts at considerably larger wavelengths. It is surely possible to obtain a better quantitative agreement with


dx.doi.org/10.1021/am405436d | ACS Appl. Mater. Interfaces 2014, 6, 2884−2892

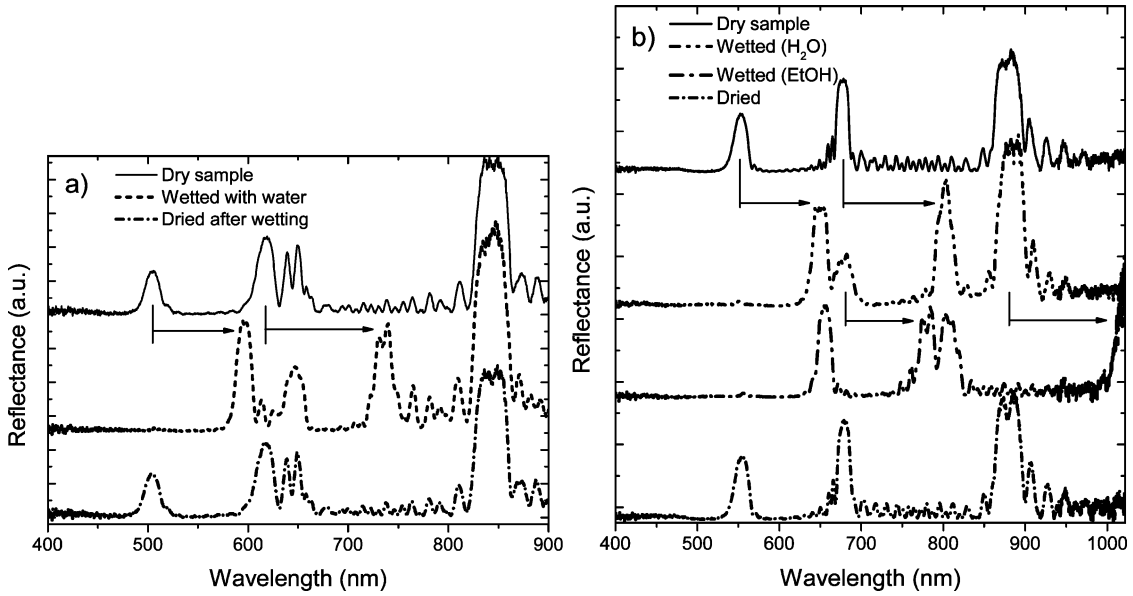


**Figure 7.** Reflectance spectra for stratified TC/THC optical structures composed of two superimposed rugate filters. A sample with four reflectance bands with two bands associated with the TCPSi layer (a). The bands originating from the TCPSi layer undergo a reversible red shift when the structure is wetted with water. With slight modification of preparation parameters, two bands can be made to overlap, leading to a structure that exhibits only three reflectance bands (b). Wetting with water or ethanol will shift the reflectance bands, leading to splitting of the overlapping reflectance bands. Band shifts induced by fluidic infiltration are indicated with small arrows. The band splitting is reversed as the adsorbate molecules desorb from the pores. Upon ethanol exposure, we see that the reflectance band located around 900 nm is shifted so that it is partially out of the spectrometers range.

more rigorous modelling that would properly take dispersion into account, but since we are only using simulations for obtaining a qualitative description for the liquid-infiltration process, we resorted to a simplified approximation. To correct the shift of the second reflectance band, we took dispersion into account with the following correction. The reflectance band originating from the THCPSi layer is located near 800 nm, and the refractive index of silicon in this wavelength region is quite different compared to 589 nm. If we make a dispersion-related correction to the THCPSi layer and use a refractive-index value appropriate for Si at 800 nm ($n_{Si}$ = 3.66), then we find that our simulation matches the experimental results much more accurately (Figure 5c). Even though the simulations presented here by no means constitute a rigorous mathematical modelling of the optical behavior, this simplified model still gives us a great qualitative description that coincides well with the experimental results. Direct comparison of experimental and simulated spectra is shown in Figure S4.

**Stacking of Superimposed Rugate Filters.** After demonstrating the basic functionality of the TC/THC-stacking method, we applied it for creating more complex optical structures. This was accomplished by preparing rugate filters with a refractive-index profile composed of a superposition of two sine waves, in succession. The outcome is a filter that produces a reflectance spectrum with four reflectance bands: two bands from both layers. Figure 6 shows cross-sectional SEM images taken from a rugate structure where a dual-band THCPSi rugate filter was prepared below a dual-band TCPSi filter. The magnified view of the interface region between the stacked filters shows the morphology of the porous structure. Even though some larger pores are present at the vicinity of the interface region, no cracking was observed and the filter remained intact.

Reflectance spectra for the stratified structure are shown in Figure 7a. The functionality of the TC/THC structure is demonstrated again, and we see that the reflectance bands associated with the TCPSi layer are red-shifted upon water intake. This serves as proof that it is possible to create complicated stratified optical filters with the TC/THC functionality. More importantly, this enables the creation of interesting novel photonic structures. For instance, by slightly modifying the preparation parameters for the structure shown in Figure 7a, we can make two reflective bands originating from successive PSi layers overlap. As a result, we have a spectrum with three bands (Figure 7b). The interesting aspect in this structure is that we are now able to split the overlapping reflectance bands by infiltrating the TCPSi layer with water. The reflectance spectrum recorded for the wetted sample displays four reflectance bands (Figure 7b). In the case of ethanol infiltration, we can see that all bands shift as the entire structure is wetted with ethanol. Despite the fact that ethanol infiltrates both layers, the overlapping reflectance bands are again split into two separate bands. This can be attributed to differing periodicities in the TCPSi and THCPSi layers.

The reflectance bands originating from the upper TCPSi layer undergo a blue shift during preparation of the lower THCPSi filter (Figure S5). The reason for this might be minor additional dissolution of the TCPSi layer during the anodization process. In addition, the removal of the surface oxide layer by HF has an effect. Regardless of the reason for the slight blue shift in the reflectance bands during fabrication, the outcome is that the stratified layers creating the overlapping reflective bands have differing average refractive indices and periodicities, which lead to the splitting of the band even in the case of ethanol infiltration.

## CONCLUSIONS

We have demonstrated the preparation of stratified optical structures from PSi with a layered TC/THC surface

composition. The differing surface modifications result in significant differences in the adsorption properties of the respective layers, and enable us to shift reflectance bands selectively by infiltrating the porous structure partially or completely, by selecting an appropriate liquid adsorbate. Moreover, the TC/THC stratified filters exhibit superior hydrolytic stability, making it the only surface chemistry combination for PSi that has been so far demonstrated as feasible for long-term applications involving repeated liquid infiltration. Although the behavior of the stratified structure changes upon aging, this does not affect the functionality of the structure. The aging phenomenon is attributed to surface oxidation of the TCPSi layer. The adsorption behavior of fresh and aged samples can be explained qualitatively with modelling based on the transfer matrix method and the Bruggeman EMA, which makes the changes predictable during extended use over a longer period of time. The present work also demonstrates that with proper chemical stabilization it is possible to activate passive optical elements based on PSi with fluidic infiltration in a controlled manner without loss of functionality over extended periods of time.

## EXPERIMENTAL SECTION

**Materials.** Boron-doped monocrystalline (100) silicon wafers with 0.01−0.02 and 0.005−0.03 Ω cm resistivity were acquired from Electronics and Materials Corporation Limited and Ferrotec Silicon Corporation, respectively. Aqueous HF (46−48 wt %) was purchased from Stella Chemifa Corp. Ethanol was purchased from Nacalai Tesque, Inc. 1-Decene was acquired from Sigma-Aldrich, and undecylenic acid (10-undecenoic acid) and aqueous NaOH (1 M) were from Merck.

**Sample Anodization.** Porous silicon was prepared by electrochemical anodization of *p*-type (100) Si wafers. The electrolyte solution was composed of hydrofluoric acid (46−48 wt %) and ethanol in a 1:1.7 volumetric ratio. A Teflon cell with 0.79 $cm^2$ anodization area was used for sample preparation. Anodization current profiles were generated with a programmable current source (Keithley 6221), and current was passed between a Pt counter electrode and a Cu current collector, which was placed in contact with the Si working electrode. Electrical contact was ensured by applying a InGa eutectic on the backside of the Si electrode. Quintic refractive-index matching layers according to Southwell[31] were added on the air-PSi and PSi-Si interfaces. The air-PSi quintic layer was anodized for 9 s with an anodization current density ranging from 126.6 to 88.6 mA $cm^{-2}$. The second quintic layer at the PSi-Si interface was anodized for 18 s from 88.6 to 0 mA $cm^{-2}$. The rugate filters were anodized with an average anodization current density of 88.6 mA $cm^{-2}$. The sine wave amplitude was varied between 12.7 and 6.3 mA $cm^{-2}$, and the period lengths were varied between 3 and 6 s.

**Surface Treatments.** Thermal carbonization (TC) was conducted after the preparation of the first porous layer. The samples were removed from the electrochemical cell and dried carefully under an argon flow. The dried samples were placed in a quartz tube and kept under constant $N_2$ flow (1 L $min^{-1}$) for a minimum of 30 min. Acetylene flow was introduced in tandem with the $N_2$ flow (1:1 by volume) for 10 min. The acetylene flow was cut off, and after a 30 s delay, the quartz tube was inserted to a tube furnace, set at 700 °C, for 10 min. After the heat treatment, the samples were allowed to cool to room temperature under a $N_2$ flow. The second filter layer was created under the TCPSi layer with standard electrochemical anodization by inserting the samples back into the electrochemical cell. After the preparation of the second layer, the samples were removed from the cell and dried under an argon flow. The THC treatment was conducted by inserting the dried samples into a quartz tube and subjecting the samples to a constant $N_2$ flow (1 L $min^{-1}$) for a minimum of 30 min. Acetylene flow was introduced in tandem with the $N_2$ flow (1:1 by volume) for 10 min, and the quartz tube was then inserted to a tube furnace, set at 500 °C, for 10 min. The acetylene flow was cut off 30 s before removing the quartz tube from the furnace, and the samples were allowed to cool to room temperature under a $N_2$ flow.

Thermal hydrosilylation was conducted by immersing freshly prepared samples into neat undecylenic acid or 1-decene solution and heating the samples at 120 °C for 22 h in an inert atmosphere. After the hydrosilylation treatment, the samples were washed copiously with ethanol and dichloromethane to remove unreacted hydrocarbon species. Thermal oxidation was conducted under ambient atmospheric conditions by inserting freshly prepared samples in an oven set at 300 °C for 2 h.

**Sample Characterization.** Reflectance measurements were conducted with an Ocean Optics HR4000CG-UV-NIR spectrometer. A tungsten halogen lamp was used as the light source (LS-1, Ocean Optics). The reflectance spectra were acquired by illuminating the samples at a normal angle of incidence. The morphology of the samples was investigated with scanning electron microscopy (JEOL JSM-6500FE), employing secondary electron imaging. Time-lapse photography was conducted with a digital camera (Nikon D5100).

## ASSOCIATED CONTENT

### Supporting Information

Simulations with the transfer matrix method, cross-sectional SEM images, values for the extinction coefficient used in simulations, direct comparison of experimental and simulated reflectance spectra, and evolution of reflectance spectra during sample preparation. This material is available free of charge via the Internet at http://pubs.acs.org.

## AUTHOR INFORMATION

### Corresponding Author

*E-mail: tero.jalkanen@utu.fi.

### Author Contributions

The manuscript was written through contributions of all authors. All authors have given approval to the final version of the manuscript.

### Notes

The authors declare no competing financial interest.

## ACKNOWLEDGMENTS

This work was partially supported by a Grant-in-Aid from the Japan Society for the Promotion of Science for Scientific Research (B) under grant no. 22350092. T.J. acknowledges financial support from MEXT, the Japanese Ministry of Education, Culture, Sports, Science & Technology, the Emil Aaltosen Säätiö, and the Scandinavia-Japan Sasakawa Foundation.

## REFERENCES

(1) De Stefano, L.; Orabona, E.; Lamberti, A.; Rea, I.; Rendina, I. Microfluidics Assisted Biosensors for Label-Free Optical Monitoring of Molecular Interactions. *Sens. Actuators, B* **2013**, *179*, 157−162.

(2) Erickson, D.; Rockwood, T.; Emery, T.; Scherer, A.; Psaltis, D. Nanofluidic Tuning of Photonic Crystal Circuits. *Opt. Lett.* **2006**, *31*, 59−61.

(3) Jane, A.; Dronov, R.; Hodges, A.; Voelcker, N. H. Porous Silicon Biosensors on the Advance. *Trends Biotechnol.* **2009**, *27*, 230−239.

(4) Snow, P. A.; Squire, E. K.; Russell, P.; St, J.; Canham, L. T. Vapor Sensing Using the Optical Properties of Porous Silicon Bragg Mirrors. *J. Appl. Phys.* **1999**, *86*, 1781−1784.

(5) De Stefano, L.; Moretti, L.; Lamberti, A.; Longo, O.; Rocchia, M.; Rossi, A. M.; Arcari, P.; Rendina, I. Optical Sensors for Vapors, Liquids, and Biological Molecules Based on Porous Silicon Technology. *IEEE Trans. Nanotechnol.* **2004**, *3*, 49−54.

(6) King, B. H.; Ruminski, A. M.; Snyder, J. L.; Sailor, M. J. Optical-Fiber-Mounted Porous Silicon Photonic Crystals for Sensing Organic Vapor Breakthrough in Activated Carbon. *Adv. Mater.* **2007**, *19*, 4530−4534.
(7) Rong, G.; Najmaie, A.; Sipe, J. E.; Weiss, S. M. Nanoscale Porous Silicon Waveguide for Label-Free DNA Sensing. *Biosens. Bioelectron.* **2008**, *23*, 1572−1576.
(8) Vincent, G. Optical Properties of Porous Silicon Superlattices. *Appl. Phys. Lett.* **1994**, *64*, 2367−2369.
(9) Berger, M. G.; Arens-Fischer, R.; Thönissen, M.; Krüger, M.; Billat, S.; Lüth, H.; Hilbrich, S.; Theiß, W.; Grosse, P. Dielectric Filters Made of PS: Advanced Performance by Oxidation and New Layer Structures. *Thin Solid Films* **1997**, *297*, 237−240.
(10) Birner, A.; Wehrspohn, R. B.; Gösele, U. M.; Busch, K. Silicon-Based Photonic Crystals. *Adv. Mater.* **2001**, *13*, 377−388.
(11) Lin, V. S.; Motesharei, K.; Dancil, K.-P. S.; Sailor, M. J.; Ghadiri, M. R. A Porous Silicon-Based Optical Interferometric Biosensor. *Science* **1997**, *278*, 840−843.
(12) Janshoff, A.; Dancil, K. S.; Steinem, C.; Greiner, D. P.; Lin, V. S.-Y.; Gurtner, C.; Motesharei, K.; Sailor, M. J.; Ghadiri, M. R. Macroporous p-Type Silicon Fabry−Perot Layers. Fabrication, Characterization, and Applications in Biosensing. *J. Am. Chem. Soc.* **1998**, *120*, 12108−12116.
(13) Jalkanen, T.; Mäkilä, E.; Suzuki, Y.-I.; Urata, T.; Fukami, K.; Sakka, T.; Salonen, J.; Ogata, Y. H. Studies on Chemical Modification of Porous Silicon-Based Graded-Index Optical Microcavities for Improved Stability under Alkaline Conditions. *Adv. Funct. Mater.* **2012**, *22*, 3890−3898.
(14) Ruminski, A. M.; King, B. H.; Salonen, J.; Snyder, J. L.; Sailor, M. J. Porous Silicon-Based Optical Microsensors for Volatile Organic Analytes: Effect of Surface Chemistry on Stability and Specificity. *Adv. Funct. Mater.* **2010**, *20*, 2874−2883.
(15) Buriak, J. M. Organometallic Chemistry on Silicon and Germanium Surfaces. *Chem. Rev.* **2002**, *102*, 1271−1308.
(16) Salonen, J.; Björkqvist, M.; Laine, E.; Niinistö, L. Stabilization of Porous Silicon Surface by Thermal Decomposition of Acetylene. *Appl. Surf. Sci.* **2004**, *225*, 389−394.
(17) Björkqvist, M.; Salonen, J.; Laine, E. Humidity Behavior of Thermally Carbonized Porous Silicon. *Appl. Surf. Sci.* **2004**, *222*, 269−274.
(18) Torres-Costa, V.; Martín-Palma, R. J.; Martínez-Duart, J. M.; Salonen, J.; Lehto, V.-P. Effective Passivation of Porous Silicon Optical Devices by Thermal Carbonization. *J. Appl. Phys.* **2008**, *103*, 083124-1−083124-4.
(19) Link, J. R.; Sailor, M. J. Smart Dust: Self-Assembling, Self-Orienting Photonic Crystals of Porous Si. *Proc. Natl. Acad. Sci. U.S.A.* **2003**, *100*, 10607−10610.
(20) Ruminski, A. M.; Moore, M. M.; Sailor, M. J. Humidity-Compensating Sensor for Volatile Organic Compounds Using Stacked Porous Silicon Photonic Crystals. *Adv. Funct. Mater.* **2008**, *18*, 3418−3426.
(21) Song, J. H.; Sailor, M. J. Chemical Modification of Crystalline Porous Silicon Surfaces. *Comments Inorg. Chem.* **1999**, *21*, 69−84.
(22) Ciampi, S.; Böcking, T.; Kilian, K. A.; Harper, J. B.; Gooding, J. J. Click Chemistry in Mesoporous Materials: Functionalization of Porous Silicon Rugate Filters. *Langmuir* **2008**, *24*, 5888−5892.
(23) De Stefano, L.; Rea, I.; Giardina, P.; Armenante, A.; Rendina, I. Protein-Modified Porous Silicon Nanostructures. *Adv. Mater.* **2008**, *20*, 1529−1533.
(24) Lehmann, V. *The Electrochemistry of Silicon*; Wiley-VCH: Weinheim, Germany, 2002.
(25) Gunning, W. J.; Hall, R. L.; Woodberry, F. J.; Southwell, W. H.; Gluck, N. S. Codeposition of Continuous Composition Rugate Filters. *Appl. Opt.* **1989**, *28*, 2945−2948.
(26) Bovard, B. G. Rugate Filter Theory: An Overview. *Appl. Opt.* **1993**, *32*, 5427−5442.
(27) Lorenzo, E.; Oton, C. J.; Capuj, N. E.; Ghulinyan, M.; Navarro-Urrios, D.; Gaburro, Z.; Pavesi, L. Porous Silicon-Based Rugate Filters. *Appl. Opt.* **2005**, *44*, 5415−5421.
(28) Dhar, S.; Seitz, O.; Halls, M. D.; Choi, S.; Chabal, Y. J.; Feldman, L. C. Chemical Properties of Oxidized Silicon Carbide Surfaces Upon Etching in Hydrofluoric Acid. *J. Am. Chem. Soc.* **2009**, *131*, 16808−16813.
(29) Mäkilä, E.; Bimbo, L. M.; Kaasalainen, M.; Herranz, B.; Airaksinen, A. J.; Heinonen, M.; Kukk, E.; Hirvonen, J.; Santos, H. A.; Salonen, J. Amine Modification of Thermally Carbonized Porous Silicon with Silane Coupling Chemistry. *Langmuir* **2012**, *28*, 14045−14054.
(30) Schoell, S. J.; Sachsenhauser, M.; Oliveros, A.; Howgate, J.; Stutzmann, M.; Brandt, M. S.; Frewin, C. L.; Saddow, S. E.; Sharp, I. D. Organic Functionalization of 3C-SiC Surfaces. *ACS Appl. Mater. Interfaces* **2013**, *5*, 1393−1399.
(31) Southwell, W. H.; Hall, R. L. Rugate Filter Sidelobe Suppression Using Quintic and Rugated Quintic Matching Layers. *Appl. Opt.* **1989**, *28*, 2949−2951.
(32) Jalkanen, T.; Salonen, J.; Torres-Costa, V.; Fukami, K.; Sakka, T.; Ogata, Y. H. Structural Considerations on Multistopband Mesoporous Silicon Rugate Filters Prepared for Gas Sensing Purposes. *Opt. Express* **2011**, *19*, 13291−13305.
(33) Macleod, H. A. *Thin-Film Optical Filters*, 2nd ed; Macmillan Publishing Co.: New York, 1986.
(34) Bruggeman, D. A. G. Berechnung Verschiedener Physikalischer Konstanten von Heterogenen Substanzen. *Ann. Phys.* **1935**, *24*, 636−679.
(35) Bergman, D. J. The Dielectric Constant of a Composite material−A Problem in Classical Physics. *Phys. Rep.* **1978**, *43*, 377−407.
(36) Polyanskiy, M. *Refractive Index Database*. http://refractiveindex.info/ (accessed Feb 1, 2013).
(37) Salem, M. S.; Sailor, M. J.; Sakka, T.; Ogata, Y. H. Electrochemical Preparation of a Rugate Filter in Silicon and Its Deviation from the Ideal Structure. *J. Appl. Phys.* **2007**, *101*, 063503-1−063503-6.
(38) Bosch, S.; Ferré-Borrull, J.; Leinfellner, N.; Canillas, A. Effective Dielectric Function of Mixtures of Three or More Materials: A Numerical Procedure for Computations. *Surf. Sci.* **2000**, *453*, 9−17.